The Driving-Force Dependence of Electrochemical Rate Parameters: Origins of Anodic–Cathodic Asymmetries for Metal–Aquo Redox Couples

Joseph T. Hupp and Michael J. Weaver*

Department of Chemistry, Purdue University, West Lafayette, Indiana 47907 *(Received: April 30, 1984)*

The consequences of differences in the intramolecular force constants and the ionic entropies between the oxidized and reduced states of aquo redox couples upon their electrochemical kinetics are examined as a function of the driving force. A generalized harmonic oscillator model is utilized that involves estimating the activation barrier from the individual force constants in the oxidized and reduced states rather than employing average ("reduced") values. Noticeable asymmetry in the anodic and cathodic Tafel plots is predicted for redox couples having large (ca. twofold) differences in force constants, the plots being more curved at anodic overpotentials. The calculated plots are in reasonable agreement with experimental Tafel plots determined previously for $Cr(OH_2)_6^{3+/2+}$ and $Eu(OH_2)_n^{3+/2+}$ at the mercury–aqueous interface. Comparisons are also presented between electrochemical "ideal" activation parameters determined for $Cr(OH_2)_6^{3+/2+}$ as a function of anodic and cathodic overpotentials and the corresponding parameters calculated from structural and thermodynamic data. Substantially smaller activation enthalpies are observed for $Cr(OH_2)_6^{2+}$ oxidation than for $Cr(OH_2)_6^{3+}$ reduction; both are close to the theoretical predictions. The anodic activation enthalpies approach zero at moderate overpotentials even though the activation entropies remain large and negative. Parallels are also drawn with corresponding results and data interpretations of the driving-force dependencies for related homogeneous reactions.

Introduction

We have recently reported and discussed an anomalous driving-force dependence of rate constants for the outer-sphere electrochemical reduction and oxidation involving metal(III/II) aquo couples of chromium, vanadium, and europium at the mercury–aqueous interface.[1,2] The metal(III) reductions exhibit linear variations of the logarithm of the work-corrected rate constant, k_{cor}, with electrode potential (i.e. Tafel plots) over the entire accessible range of overpotentials (ca. 300–600 mV, depending on the reaction).[1,3] In contrast, the work-corrected Tafel plots for the corresponding metal(II) oxidations in hexafluorophosphate or perchlorate electrolytes are sharply curved at moderate overpotentials, yielding variations of log k_{cor} with electrode potential at higher oxidation driving forces that are unexpectedly small[1] in comparison with the predictions of the usual harmonic oscillator treatment.[4] Similarly weak dependencies of the rate constants upon the thermodynamic driving force have been noted for a number of homogeneous bimolecular reactions involving oxidation of M(II) aquo complexes.[2,5-8]

The observed marked asymmetry of the anodic and cathodic Tafel plots contrasts the essentially symmetrical behavior predicted by the conventional theoretical relationships.[1] We have speculated that the major source of this asymmetry is associated with major differences in the short-range solvent polarization between the oxidized and reduced aquo species, possibly associated with a rearrangement step either before or after electron transfer.[1] However, the recent acquisition of reliable Raman spectral measurements for both M(III) and M(II) aquo complexes[9] along with the emergence of new metal–ligand bond length data[10] has prompted us to reexamine this problem. Specifically, these data indicate that the force constants for the totally symmetric metal–aquo stretching mode are expected to differ substantially (ca. twofold) between the oxidized and reduced forms for couples such as $Cr(OH_2)_6^{3+/2+}$ which feature large changes (~0.15–0.2 Å) in the metal–ligand bond lengths, Δa. Such force constant differences will yield noticeably different free energy parabolas for the oxidized and reduced forms for these reactions since a large portion of the free energy barrier is associated with inner-shell (i.e. metal–ligand) reorganization. Such asymmetry in the free energy curves for individual redox couples will often cancel for homogeneous reactions, especially those involving a structurally similar pair of redox couples. However, it can in principle yield significantly asymmetric activation energy–driving force (and hence log k_{cor}–potential) plots for electrochemical reactions at anodic and cathodic overpotentials.[4] The extent of such asymmetry has been shown to be only minor at small overpotentials.[4] We have stated previously that this factor is much too small to account for the observed Tafel plot asymmetry.[1] However, more detailed consideration of the inner-shell reaction energetics on the basis of the recent structural data leads us to revise this conclusion.

The purpose of this article is to examine in quantitative terms the predicted influence of differing metal–ligand force constants on such driving-force dependencies and the degree to which the experimental data can be accounted for on this basis. In addition, the electrochemical activation parameters for $Cr(OH_2)_6^{3+/2+}$ and $Eu(OH_2)_n^{3+/2+}$ have been evaluated over a wide range of anodic and cathodic overpotentials and are compared with the corresponding theoretical predictions. Besides providing a more complete description of the driving-force-dependent reaction energetics, such comparisons are of particular interest since the large (ca. 200 J deg^{-1} mol^{-1}) differences in entropy between the oxidized and reduced aquo cations[11] yield very substantial differences in the redox thermodynamics at anodic and cathodic overpotentials.[1] Finally, some commonalities are explored between the driving-force dependence of redox reactivities for electrochemical and homogeneous processes.

Driving-Force Dependence of Electrochemical Rate Constants

Figures 1 and 2 contain experimental Tafel plots for $Cr(OH_2)_6^{3+/2+}$ and $Eu(OH_2)_n^{3+/2+}$, respectively, over a range of anodic and cathodic overpotentials at the mercury–aqueous interface. These plots, which are taken from ref 1, are shown as solid curves. Similar data have also been obtained for $V(OH_2)_6^{3+/2+}$, although over a somewhat smaller overpotential range.[1] The dotted lines in Figures 1 and 2 are the Tafel plots

(1) Tyma, P. D.; Weaver, M. J. *J. Electroanal. Chem. Interfacial Electrochem.* **1980**, *111*, 195.
(2) Weaver, M. J.; Hupp, J. T. *ACS Symp. Ser.* **1982**, *No. 198*, 181.
(3) Weaver, M. J.; Anson, F. C. *J. Phys. Chem.* **1976**, *80*, 1861.
(4) Marcus, R. A. *J. Chem. Phys.* **1965**, *43*, 679.
(5) Chou, M.; Creutz, C.; Sutin, N. *J. Am. Chem. Soc.* **1977**, *99*, 5615.
(6) Creutz, C. *Inorg. Chem.* **1978**, *17*, 1046.
(7) Weaver, M. J.; Yee, E. L. *Inorg. Chem.* **1980**, *19*, 1936.
(8) Balzani, V.; Scandola, F.; Orlandi, G.; Sabbatini, N.; Indelli, M. T. *J. Am. Chem. Soc.* **1981**, *103*, 3370.
(9) (a) Best, S. P.; Beattie, J. K.; Armstrong, R. S. *J. Chem. Soc., Dalton Trans.*, in press. (b) Jenkins, T. E.; Lewis, J. *Spectrochim. Acta, Part A* **1981**, *37A*, 47.
(10) Brunschwig, B. S.; Creutz, C.; MaCartney, D. H.; Sham, T. K.; Sutin, N. *Faraday Discuss. Chem. Soc.* **1982**, *No. 74*, 113.
(11) Yee, E. L.; Cave, R. J.; Guyer, K. L.; Tyma, P. D.; Weaver, M. J. *J. Am. Chem. Soc.* **1979**, *101*, 1131.

0022-3654/84/2088-6128$01.50/0

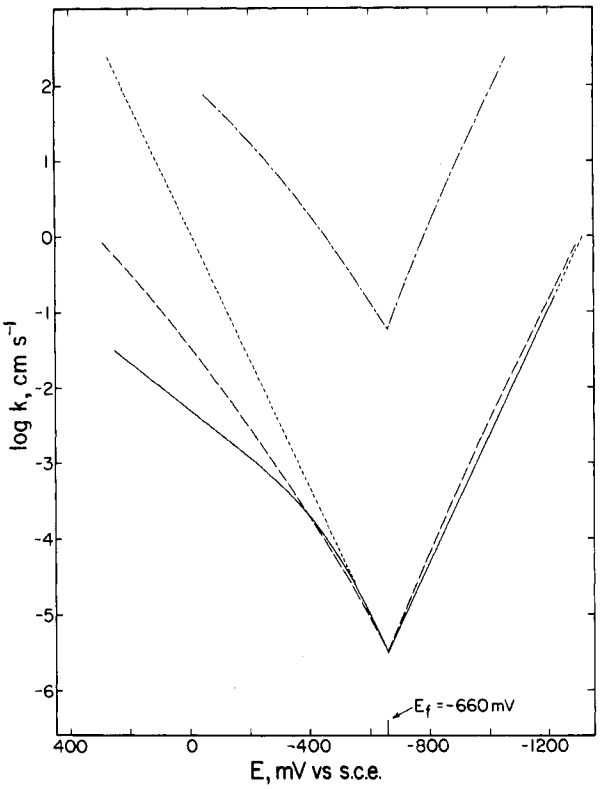

Figure 1. Plots of the logarithm of the rate constant, log k, for $Cr(OH_2)_6^{3+}$ reduction and $Cr(OH_2)_6^{2+}$ oxidation at cathodic and anodic overpotentials, respectively, against the electrode potential, E. Solid curves are the experimental work-corrected Tafel plots at the mercury–aqueous interface, taken from ref 1 and 3. The dotted line is the anodic Tafel plot corresponding to a transfer coefficient of 0.50. (Experimental cathodic Tafel plot has a slope of 0.50.) Dashed lines are anodic and cathodic Tafel plots calculated by using individual force constants for Cr^{III}–OH_2 and Cr^{II}–OH_2 bonds (see text for details). Dotted-dashed curves are corresponding calculated Tafel plots, but by assuming that the outer-shell reorganization energy equals zero.

that would be obtained for the same value of k_{cor} at the formal potential, E_f (i.e. the "standard" rate constant k^s_{cor}), if the transfer coefficient, α_{cor}, equals 0.5 throughout the entire overpotential range. The transfer coefficient is defined as

$$\alpha_{cor} = \pm(RT/F)(\mathrm{d} \ln k_{cor}/\mathrm{d}E) \quad (1)$$

where the plus-minus sign refers to anodic and cathodic rate constants, respectively. The strongly asymmetric nature of the experimental anodic and cathodic Tafel plots is clearly seen by comparison with the dotted straight lines.

The conventional expression for electrochemical rate constants as a function of the overpotential[4] can be written for one-electron reactions as

$$k_{cor} = A \exp\{[-\lambda \pm F(E - E_f)]^2/4\lambda RT\} \quad (2)$$

where the plus-minus sign again refers to anodic and cathodic rate constants, A is a preexponential factor, and λ is the intrinsic reorganization energy. This last term is the free energy required to adjust the reactant nuclear coordinates so that they correspond to those of the product, but without electron transfer. The form of eq 2 clearly predicts symmetrical curved Tafel plots at anodic and cathodic overpotentials. This symmetry follows from the assumption contained in eq 2 that the force constants of the oxidized and reduced forms are equal; i.e., the reactant and product parabolas have identical shapes.

We and others have previously employed eq 2 (or equivalent relationships) for comparing the rate constant–overpotential dependence with the harmonic oscillator model.[1,3,12] It is conventional to determine λ from the experimental standard rate constant via eq 2 and to reinsert this quantity into eq 2 to find the predicted overpotential dependence of log k_{cor} which is compared with the experimental data.[1,3,12] A somewhat different approach is used here whereby the predicted log k_{cor}–overpotential dependences are obtained directly from *calculated* free-energy barriers derived from the known redox structural parameters. This latter procedure is now outlined.

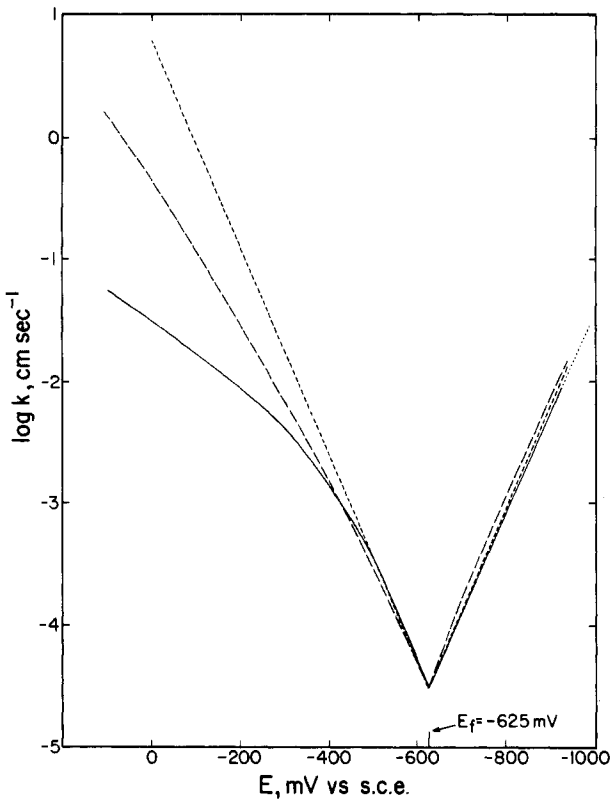

Figure 2. As Figure 1, but for $Eu(OH_2)_n^{3+/2+}$.

The work-corrected rate constant can be expressed as[13]

$$k_{cor} = K_0 \nu_n \Gamma_n \kappa_{el} \exp(-\Delta G^*/RT) \quad (3)$$

where K_0 is the statistical part of the equilibrium constant for forming the precursor state from the bulk reactant, ν_n is the nuclear frequency factor, Γ_n is the nuclear tunneling factor, κ_{el} is the electronic transmission coefficient, and ΔG^* is the free energy of activation for the elementary electron-transfer step. Although the preexponential factors exert important influences upon the absolute magnitudes of k_{cor}, the dependence of k_{cor} upon the driving force is expected to arise almost entirely from variations in ΔG^*. For the present purpose, it is particularly convenient to formulate ΔG^* in terms of intrinsic reorganization energies for the forward and reverse directions, λ_f and λ_r, respectively, for the generalized reaction

$$\mathrm{Ox.} + e^- \rightleftharpoons \mathrm{Red.} \quad (4)$$

Provided that the free energy–reaction coordinate profiles are quadratic in nature, values of ΔG^* as a function of the free energy driving force ΔG° ($= \pm F(E - E_f)$) can be obtained from the simultaneous solution to the following relations:[14]

$$\Delta G^* = \lambda_f X^2 \quad (5a)$$

(12) For example: (a) Garreau, D.; Saveant, J. M.; Tessier, D. *J. Phys. Chem.* **1979**, *83*, 3003. (b) Corrigan, D. A.; Evans, D. H. *J. Electroanal. Chem. Interfacial Electrochem.* **1980**, *106*, 287.

(13) Hupp, J. T.; Weaver, M. J. *J. Electroanal. Chem. Interfacial Electrochem.* **1983**, *152*, 1.

(14) Equations 5a and 5b define the intersection point of a pair of intersecting parabolas with differing shapes (Figure 3) being displaced vertically by an amount equal to the driving force ΔG°. This treatment is most appropriate for calculating ΔG^* for electrochemical reactions since the reactant and product parabolas refer to a *single* species rather than to homogeneous processes where a *pair* of reacting species are involved. Analogous considerations have also been made for proton-transfer processes. See: Koeppl, G. W.; Kresge, A. J. *J. Chem. Soc., Chem. Commun.* **1973**, 371. Kresge, A. J. *Chem. Soc. Rev.* **1973**, *2*, 475.

and

$$\lambda_f X^2 = \lambda_r(1 - X)^2 + \Delta G^\circ \quad (5b)$$

and X is a dimensionless parameter characterizing the nuclear coordinates of the transition state[15] (see Figure 3). (For convenience, quantities such as λ_f, ΔG^*, ΔG°, etc. refer here and below to the forward reaction, either cathodic or anodic, being considered even though the reduction process is commonly regarded as the "forward reaction", as in eq 4.) The combination of eq 3 and 5 yields the simplified symmetrical relation eq 2 only for the special case when $\lambda_f = \lambda_r = \lambda$. However, when $\lambda_f \neq \lambda_r$, they instead predict *nonsymmetrical* log k_{cor}–overpotential plots in the anodic and cathodic directions. The latter will clearly apply when the force constants differ in the oxidized and reduced forms.

The various components of eq 3 and 5 can be evaluated (or estimated) as follows. The forward and reverse reorganization energies for eq 4 can be separated into inner-shell (reactant bond distortional) and outer-shell (solvent reorganization) contributions according to

$$\lambda_f = \lambda_{is}^f + \lambda_{os} \quad (6a)$$

$$\lambda_r = \lambda_{is}^r + \lambda_{os} \quad (6b)$$

where λ_{is}^f and λ_{is}^r are the inner-shell reorganization energies associated with the reactant and product species, respectively.

These can be related to the corresponding force constant, f_i, for symmetrical bond stretching (or compression) of the ith bond, and the change in bond distance between the oxidized and reduced forms by means of

$$\lambda_{is} = 0.5\sum f_i \Delta a^2 \quad (7a)$$

where

$$f_i = 4\nu_{in}^2\pi^2c^2\mu \quad (7b)$$

where ν_{in} is the bond vibrational frequency, c is the velocity of light, and μ is the reduced mass of the vibrator.

The outer-shell reorganization energy, λ_{os}, will be assumed to be equal in the oxidized and reduced forms (vide infra). It is conventionally given by[4]

$$\lambda_{os} = \frac{e^2N}{2}\left(\frac{1}{r} - \frac{1}{R}\right)\left(\frac{1}{\epsilon_{op}} - \frac{1}{\epsilon_s}\right) \quad (8)$$

where e is the electronic charge, N is Avogadro's number, r is the reactant radius, R is the distance from the reactant to its image in the metal surface, and ϵ_{op} and ϵ_s are the optical and static dielectric constants, respectively. For the present aquo reactants, r was taken as 3.25 Å[10] and R as 13 Å.[16]

Values of ΔG^* for the $Cr(OH_2)_6^{3+/2+}$ couple were calculated as a function of overpotential from eq 5–8, with μ taken as the mass of the aquo ligand, along with the experimental values ν_{III} = 543 cm^{-1}, $\nu_{II} \approx$ 380 cm^{-1},[9,17] and Δa = 0.20 Å.[10] This yields inner-shell reorganization energies, λ_{is}^f and λ_{is}^r, equal to 223 and 110 kJ mol^{-1}, respectively, and overall reorganization energies, λ_f and λ_r, of 310 and 197 kJ mol^{-1}, respectively. The corresponding calculated values of k_{cor} were obtained by combining the values of ΔG^* with numerical estimates of the preexponential factors in eq 3. Details concerning the physical significance of these quantities are given elsewhere.[13,18,19] The composite quantity $K_0\kappa_{el}$ was taken as 0.5 Å; similar values (within ca. twofold) are indicated from both experimental and theoretical lines of evidence.[20]

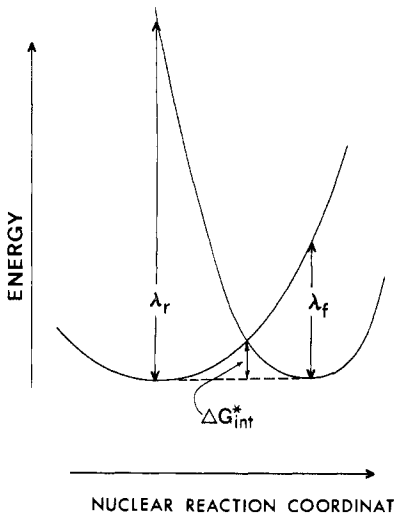

Figure 3. Schematic representation of forward and reverse reorganization energies, λ_f and λ_r, for the case when the force constants for the product bonds are greater than for the reactant bonds. The nuclear reaction coordinate is given by the dimensionless parameter X in eq 5.

The nuclear tunneling factor Γ_n was obtained from the driving-force-dependent relationship of Holstein[21] as expressed conveniently by Sutin.[22] It is calculated to equal 3.4 at $E = E_f$ and depends only slightly upon overpotential in the range of interest here. The nuclear frequency factor ν_n was determined as 1.0×10^{13} s^{-1} from the above stretching frequencies as described in ref 13.

The resulting calculated values of log k_{cor} against $(E - E_f)$ for $Cr(OH_2)_6^{3+/2+}$ in both anodic and cathodic directions are plotted as dashed curves in Figure 1. The standard rate constant, k_{cor}^s, obtained from theory is in almost exact agreement with the experimental value, 3×10^{-6} cm s^{-1}. Given the uncertainties and assumptions involved in deriving the former (probably ca. ±20-fold), this agreement is somewhat fortuitous. For convenience, the calculated and experimental values of k_{cor}^s are set exactly equal in Figure 1 so to facilitate the comparison of the theoretical predictions for the driving-force dependence of k_{cor} with experiment.

The theoretical analysis for $Eu(OH_2)_n^{3+/2+}$ cannot be performed on the same quantitative basis as for $Cr(OH_2)_6^{3+/2+}$ since experimental data for ν_{III}, ν_{II}, and Δa are unavailable. However, approximate calculations of the log k_{cor}–overpotential plots for this couple may still be carried out. From the experimental standard rate constant, $k_{cor}^s = 3 \times 10^{-5}$ cm s^{-1}, together with the theoretical value of λ_{os} assuming r = 3.5 Å and R = 13 Å (87 kJ mol^{-1}, eq 8) and noting that the reaction is likely to be nearly adiabatic ($\kappa_{el} \sim 1$),[23] an intrinsic inner-shell barrier, ΔG^*_{int} (i.e. ΔG^* for $\Delta G^\circ = 0$), of ca. 30 kJ mol^{-1} is inferred. Since the interaction of Eu(III) and Eu(II) with the aquo ligands is predominantly electrostatic, the Eu–OH_2 force constants should be approximately proportional to the ionic charge divided by the cation–aquo bond distance, a.[24] Given that a is likely to be about 2 Å and the difference in bond lengths between Eu(III)–OH_2 and Eu(II)–OH_2 is around 0.22 Å,[33] from the above values of ΔG^*_{int} and λ_{os} and utilizing eq 5 for $\Delta G^\circ = 0$ along with eq 6 leads to estimates of $\lambda_{in}^{Ox.}$ and $\lambda_{in}^{Red.}$ of 170 and 95 kJ mol^{-1}, respectively. The overpotential dependence of log k_{cor} for $Eu(OH_2)_n^{3+/2+}$ predicted by these parameters is shown as dashed curves in Figure 2.

Comparison between the experimental and calculated Tafel plots for $Cr(OH_2)_6^{3+/2+}$ and $Eu(OH_2)_n^{3+/2+}$ in Figures 1 and 2 reveals that the observed anodic–cathodic asymmetry is accounted

(15) The parameters X (eq 5) and α (eq 1) provide two distinct descriptions of the transition-state symmetry: the former indicates the location of the transition state along the reaction coordinate associated with changes in nuclear configuration (Figure 3), whereas the latter describes the effective fractional ionic charge in the transition state. In the harmonic oscillator model, α and X are equal at all points if $\lambda_f = \lambda_r$ (and are also equivalent to Marcus' $-m$ parameter[4]). However, this is not the case for the reactions described here since $\lambda_f \neq \lambda_r$.

(16) Weaver, M. J. *J. Phys. Chem.* **1980**, *84*, 568.

(17) Although the average symmetric Cr(II)–O stretching frequency in $Cr(OH_2)_6^{2+}$ has not been measured directly, it is likely to be close to 380 cm^{-1} on the basis of similar values for several divalent metal–aquo complexes.[10]

(18) Hupp, J. T. Ph.D. Dissertation, Michigan State University, 1983.

(19) Hupp, J. T.; Weaver, M. J., submitted for publication.

(20) Hupp, J. T.; Weaver, M. J. *J. Phys. Chem.* **1984**, *88*, 1463.

(21) Holstein, T.; Sher, H. *Philos. Mag.*, [*Part*] *B.* **1981**, *44*, 343.

(22) Sutin, N. *Prog. Inorg. Chem.* **1983**, *30*, 441.

(23) Yee, E. L.; Hupp, J. T.; Weaver, M. J. *Inorg. Chem.* **1983**, *22*, 3465.

(24) Bockris, J. O'M.; Reddy, A. K. N. "Modern Electrochemistry"; Plenum Press: New York, 1970; Vol. I, Chapter 2.

TABLE I: Dependence of Experimental and Calculated Transfer Coefficients for $Cr(OH_2)_6^{3+/2+}$ on Anodic As Compared to Cathodic Overpotentials

$\pm(E - E_f)$,[a] mV	anodic		cathodic		
	α_{cor}^{a} [b]	α_{calcd}^{a} [c]	α_{cor}^{c} [d]	α_{calcd}^{c} [e]	α_{calcd}^{sym} [f]
0		0.45		0.55	0.50
200	0.35	0.40	0.50	0.52	0.46
400	0.22	0.36	0.49	0.47	0.42
600	0.20	0.33	~0.48	0.43	0.38
800	~0.19	0.29			0.34

[a] Anodic or cathodic overpotential. [b] Anodic experimental transfer coefficient corrected for work terms, at listed overpotentials (data from ref 1). [c] Anodic transfer coefficient, calculated by using individual force constants for Cr^{III}–OH_2 and Cr^{II}–OH_2 bonds as described in text. [d] Cathodic experimental transfer coefficient corrected for work terms, at listed overpotentials (data from ref 3). [e] Cathodic transfer coefficient, calculated by using individual force constants for Cr^{III}–OH_2 and Cr^{II}–OH_2 bonds as described in text. [f] Anodic or cathodic transfer coefficient calculated by assuming equal force constants in oxidized and reduced forms (eq 2).

for in part by the inclusion of large force constants for the oxidized compared to the reduced forms in the theoretical calculations. Thus, these ratios of inner-shell force constants, estimated to be 2.05 and ca. 1.8 for $Cr(OH_2)_6^{3+/2+}$ and $Eu(OH_2)_n^{3+/2+}$, respectively, yield noticeably smaller slopes in the Tafel plots at anodic as compared to cathodic overpotentials. Even though the predicted Tafel plots at cathodic overpotentials do exhibit some curvature, these are nevertheless closely similar to the essentially linear experimental plots in Figures 1 and 2. At anodic overpotentials, the marked curvature in the experimental Tafel plots is roughly mimicked by the calculated plots, especially for $Cr(OH_2)_6^{2+}$ oxidation.

A comparison between the experimental and calculated transfer coefficients for $Cr(OH_2)_6^{3+/2+}$, derived from the slopes of the curves in Figure 1 (eq 1), is given in Table I. The calculated anodic and cathodic quantities, α_{calcd}^{a} and α_{calcd}^{c}, respectively, were obtained from the dashed curves, i.e. by using individual force constants. Although the changes in α_{calcd}^{a} and α_{calcd}^{c} with varying overpotential are similar, the former are substantially larger at a given overpotential, in harmony with the behavior of the corresponding experimental quantities α_{calcd}^{a} and α_{calcd}^{c} (Table I). In contrast, the transfer coefficient, α_{calcd}^{sym}, calculated from the conventional treatment (eq 2) displays a symmetrical overpotential dependence, in marked disagreement with the observed behavior (Table I).[1] The values of α_{cor}^{a} are nevertheless significantly smaller than α_{calcd}^{a} at large anodic overpotentials; this is also evident from the deviations between the solid and dashed curves in Figure 1.

These residual discrepancies between theory and experiment at anodic overpotentials may be due to several causes. Most simply, the actual curvature in the experimental log k_{cor}–E plots may be somewhat different from that shown in Figures 1 and 2 due to possible potential-dependent errors in the application of double-layer corrections to the observed rate constants. Although the extent of this uncertainty is not large (around ca. twofold in log k_{cor}), it is greatest at the largest anodic overpotentials in view of the substantial anionic specific adsorption encountered even in hexafluorophosphate electrolytes.[1] However, it is more likely that the discrepancies are due largely to remaining inadequacies of the theoretical model. One possibility is that the metal–ligand vibrational modes are anharmonic. However, trial calculations using anharmonic Morse potentials in place of the harmonic oscillator model (eq 7) yielded almost imperceptible changes in the Tafel plots, at least for the conditions encountered in Figure 1.[25] A more important factor, at least for $Cr(OH_2)_6^{3+/2+}$, is liable to reside in the above assumption that all the metal–ligand bonds are equivalent. A pair of trans chromium–oxygen bonds in $Cr(OH_2)_6^{2+}$ are expected to be weaker, and therefore have smaller force constants, than the other four due to Jahn–Teller distortion. Since these bonds are also especially elongated,[10] they may well contribute importantly to the inner-shell barrier, yielding a more pronounced curvature in the calculated anodic Tafel plot.

As noted above, we previously attributed the observed Tafel plot asymmetry chiefly to the influence of short-range solvent polarization.[1,3] Although a large fraction of the asymmetry effect now appears to reside in the inner-shell barrier, the present analysis suggests a way in which the outer-shell reorganization can contribute as well. We assumed above that λ_{os} is equal for the reduction and oxidation directions; i.e., the outer-shell "force constant" is independent of the metal oxidation state. This follows from the simple dielectric continuum model used to estimate the outer-shell barrier. If reorganization of hydrogen-bonded outer-shell water molecules contributes significantly to the free energy barrier, greater Tafel plot asymmetry should result since the effective force constants associated with such motions should also be larger in the higher oxidation state.[3] However, quantitative calculations of such effects are precluded at present due to the incompleteness of molecular structural information for the surrounding solvent.

With regard to recent provocative discussions,[26,27] we stress that it is necessary to include the outer-shell solvent contribution to the reorganization barrier in order to obtain satisfactory agreement between the theoretical and experimental rate constants for $Cr(OH_2)_6^{3+/2+}$. This is also the case for a variety of other homogeneous and electrochemical reactions.[19] To illustrate this point for $Cr(OH_2)_6^{3+/2+}$, Figure 1 also contains log k_{cor}–E plots calculated by ignoring the solvent contribution (dotted-dashed lines). Although exhibiting very similar *dependences* of log k_{cor} upon overpotential to that seen with the proper inclusion of the solvent reorganization component, the calculated values of log k_{cor} are substantially (ca. 10^4-fold) larger than the experimental values.

In view of the continuing interest and speculation concerning the virtues of Tafel plots for examining some fundamental aspects of electrochemical kinetics,[26,28,29] it is worthwhile to note some more general implications of the foregoing. It is evident that the degree of curvature of the Tafel plots can be at least as sensitive to the degree of mismatch between the forward and reverse reorganization energies as to the absolute magnitude of these energies and hence to the intrinsic barrier, ΔG^*_{int}, and to k^s_{cor}. It is therefore extremely dangerous to estimate intrinsic barriers from the curvature of Tafel plots.[28,30,31] Further, the Tafel plot shapes are not very diagnostic of the factors contributing to reactant activation, such as the role of solvent reorganization. A more valuable approach to examining such fundamental questions is to compare the absolute magnitudes of the calculated and experimental rate constants under well-defined conditions[19] rather than their dependence upon the thermodynamic driving force. Nevertheless, such Tafel comparisons do provide one means of evaluating more subtle driving-force-dependent effects with the aim of "fine tuning" theoretical formulations.

Driving-Force Dependence of Electrochemical Activation Parameters

Activation parameters clearly provide an additional measure of information on the reaction energetics beyond that yielded by rate measurements at a single temperature. These parameters can be particularly revealing, for example, of the solvational changes accompanying transition-state formation for simple redox reactions.[32] Two distinct types of activation parameters can usefully be distinguished for electrochemical reactions. The first type, the so-called "real" activation parameters, refers to the

(25) Hupp, J. T., unpublished work.

(26) Khan, S. U. M. In "Modern Aspects of Electrochemistry"; Bockris, J. O'M., Conway, R. E., White, R. E., Eds.; Plenum Press: New York, 1983; Vol. 15.
(27) Bockris, J. O'M.; Khan, S. U. M. *J. Phys. Chem.* **1983**, *87*, 4012.
(28) Bockris, J. O'M.; Khan, S. U. M. "Quantum Electrochemistry"; Plenum Press: New York, 1979; Chapter 7.
(29) Saveant, J.-M.; Tessier, D. *Faraday Discuss. Chem. Soc.* **1982**, *No. 74*, 57.
(30) Memming, R.; Mollers, F. *Ber. Bunsenges. Phys. Chem.* **1972**, *76*, 475.
(31) Fukuzumi, S.; Wong, C. L.; Kochi, J. K. *J. Am. Chem. Soc.* **1980**, *102*, 2928. Klinger, R. J.; Kochi, J. K. *J. Am. Chem. Soc.* **1981**, *103*, 5839.
(32) Weaver, J. M. *J. Phys. Chem.* **1979**, *83*, 1748.

TABLE II: Comparison of Experimental and Calculated Activation Parameters for $Cr(OH_2)_6^{3+/2+}$ at Cathodic and Anodic Overpotentials

$E^{ni} - E_f$,[a] mV	ΔH^*_{cor},[b] kJ mol^{-1}	ΔH^*_{calcd},[c] kJ mol^{-1}	ΔS^*_{cor},[d] J K^{-1} mol^{-1}	ΔS^*_{calcd},[e] J K^{-1} mol^{-1}
		$Cr(OH_2)_6^{3+}$ Reduction		
−350	63	64	68	80
−300	68	66	68	80
−250	73	70	68	82
−200	78	74	66	85
−150	84	77	65	88
		$Cr(OH_2)_6^{2+}$ Oxidation		
350	11	17	−85	−90
450	9	15	−90	−85
550	7	13	−92	−80
650	5	12	−95	−78
750	4	10	−92	−75
850	3	9	−90	−70
900	2	8	−85	−66

[a] Overpotential, where E^{ni} is the nonisothermal cell electrode potential with reference electrode held at 25° and E_f is the formal potential for $Cr(OH_2)_6^{3+/2+}$ (−660 mV) at 25 °C. [b] Experimental work-corrected "ideal" enthalpy of activation for $Cr(OH_2)_6^{3+}$ reduction (cathodic overpotentials) or $Cr(OH_2)_6^{2+}$ oxidation (anodic overpotentials). The former was evaluated with 1 M $NaClO_4$ supporting electrolyte,[32] and latter with 0.4 M KPF_6. [c] Corresponding calculated "ideal" enthalpy of activation, obtained as described in text. [d] Work-corrected ideal entropy of activation for $Cr(OH_2)_6^{3+}$ reduction (cathodic overpotentials) or $Cr(OH_2)_6^{2+}$ oxidation (anodic overpotentials), obtained from corresponding values of ΔH^*_{cor} and k_{cor} as outlined in text. [e] Corresponding calculated ideal entropy of activation, obtained as outlined in text.

temperature dependence of the rate constant measured at a fixed overpotential.[33] The second type, the so-called "ideal" activation parameters, is obtained from the temperature derivative evaluated at a fixed nonisothermal electrode potential.[32-34] The difference between these two types lies in the thermodynamic entropy change, the "reaction entropy" ΔS°_{rc}, brought about by electron transfer, i.e. the entropy difference between the reduced and oxidized forms of the redox couple.[11] This entropy change is associated with the temperature dependence of the standard electrode potential[11] and gives rise to an inherent asymmetry of the electrochemical reaction energetics in the anodic and cathodic directions. Thus, at the standard potential E_f where the free energy driving force, ΔG°, necessarily equals zero, there will nevertheless be a nonzero (and often substantial) reductive enthalpic driving force, ΔH°_{rc}, since then $\Delta H^\circ_{rc} = T\Delta S^\circ_{rc}$.[32-34] Thus, for $Cr(OH_2)_6^{3+/2+}$, $\Delta S^\circ_{rc} = 205$ J K^{-1} mol^{-1},[11] and therefore at E_f, $\Delta H^\circ_{rc} = 61$ kJ mol^{-1}. This is a key feature which sets apart electrochemical exchange reactions from the corresponding homogeneous self-exchange reactions; the latter are inherently symmetrical since they can be conceived as a coupled pair of electrochemical exchange reactions.[2]

The "ideal" activation parameters can be identified with the actual enthalpic and entropic barriers at the electrode potential at which they are evaluated. The cathodic and anodic ideal parameters will therefore differ markedly even at the standard electrode potential. The real activation parameters, on the other hand, contain a correction for the entropic driving force; they will necessarily be identical in the anodic and cathodic directions at the standard potential since the temperature-dependent anodic and cathodic rate constants will be equal under these conditions. The latter are therefore closely related to the activation parameters for homogeneous self-exchange reactions. However, the ideal parameters are more appropriate for the present purposes since they reveal the true asymmetric nature of the electrochemical reaction energetics.

Table II contains a comparison of experimental ideal enthalpies and entropies of activation, ΔH^*_{cor} and ΔS^*_{cor}, respectively, with the corresponding calculated quantities, ΔH^*_{calcd} and ΔS^*_{calcd}. The work-corrected activation enthalpies, ΔH^*_{cor}, were obtained from[35]

$$\Delta H^*_{cor} = -R[\partial \ln k_{cor}/\partial(1/T)]_{E^{ni}} \quad (9)$$

where the temperature dependence of k_{cor} is evaluated at the constant nonisothermal cell potential E^{ni}. The values of k_{cor} were evaluated over the temperature range ca. 5–50 °C; experimental details are given in ref 32. At cathodic overpotentials the k_{cor} values were obtained from apparent rate constants measured in 1 M $NaClO_4$ (pH 2.5) as outlined in ref 32. At anodic overpotentials, they were evaluated from rate data measured in 0.4 M KPF_6 (pH 2.5) as outlined in ref 1. (Since quantitative double-layer data are not available for 0.4 M KPF_6 at potentials positive of the point of zero charge (where PF_6^- specific adsorption occurs), the double-layer corrections are assumed to be independent of temperature. The approximate validity of this assumption is supported by a similar finding for $Cr(OH_2)_6^{3+}$ reduction[32] and the small absolute magnitude of the corrections required for $Cr(OH_2)_6^{2+}$ oxidation in 0.4 KPF_6.[1]) The work-corrected entropies of activation, ΔS^*_{cor}, also listed in Table II, were obtained from the corresponding values of ΔH^*_{cor} and k_{cor} at a given temperature, along with the above estimates of $K_0\kappa_{el}$ and ν_n, by using

$$\Delta S^*_{cor} = R \ln k_{cor} - R \ln (K_0\kappa_{el}\nu_n) + \Delta H^*_{cor}/T \quad (10)$$

Note that the temperature-dependent nuclear tunneling factor Γ_n is contained within ΔH^*_{cor} and ΔS^*_{cor}, so that the latter can be regarded as "semiclassical" quantities.[22]

The corresponding calculated quantities, ΔH^*_{calcd} and ΔS^*_{calcd}, were obtained as follows. As shown in the Appendix, differentiation of eq 5 with respect to temperature yields an expression for the classical activation entropy (i.e. not containing the nuclear tunneling correction):

$$\Delta S^* = \Delta S^\circ \lambda_f X[\lambda_r^2 + (\lambda_f - \lambda_r)(\Delta G^\circ + \lambda_r)]^{-1/2} \quad (11)$$

by assuming that $d\lambda_f/dT = d\lambda_r/dT = 0$,[36] where ΔS° is the entropic driving force in the cathodic or anodic direction, as appropriate. An equivalent expression for ΔS^* is simply (see Appendix)

$$\Delta S^* = \alpha \Delta S^\circ \quad (12a)$$

where the transfer coefficient, α, as operationally defined by eq 1, is calculated from

$$\alpha = \lambda_f X(X\lambda_f + \lambda_r - X\lambda_r)^{-1} \quad (12b)$$

Although eq 11 and 12 are equivalent, the latter formulation is more revealing since it separates the simple phenomenological definition of ΔS^* (eq 12a) and its detailed calculation based on a harmonic oscillator treatment for α (eq 12b).

The classical activation enthalpy, ΔH^*, is obtained from ΔS^* together with the classical activation free energy from eq 5 by using

$$\Delta H^* = \Delta G^* + T\Delta S^* \quad (13)$$

The calculated value of ΔH^*, ΔH^*_{calcd}, desired for comparison with the experimental value, ΔH^*_{cor}, is obtained by including the temperature-dependent nuclear tunneling correction:

$$\Delta H^*_{calcd} = \Delta H^* - R[d \ln \Gamma_n/d(1/T)] \quad (14)$$

Similarly, the corresponding calculated activation entropy can be obtained from

$$\Delta S^*_{calcd} = \Delta S^* - R \ln \Gamma_n - (R/T)\, d \ln\Gamma_n/d(1/T) \quad (15)$$

The resulting values of ΔH^*_{calcd} and ΔS^*_{calcd} for $Cr(OH_2)_6^{3+/2+}$ are listed alongside the corresponding experimental estimates in

(33) Weaver, M. J. *J. Phys. Chem.* **1976**, *80*, 2645.
(34) Weaver, M. J. *Isr. J. Chem.* **1979**, *18*, 35.

(35) A slightly different relation to eq 9 was employed in ref 32 (eq 3), whereby an additional ln $T^{1/2}$ term was included in the Arrhenius coefficient. This term arises from the anticipated temperature dependence of the preexponential factor on the basis of the collisional rate formalism employed in ref 32. This correction factor upon ΔH^*_{cor} is small, ca. 0.3 kcal mol^{-1}. However, we no longer consider this term appropriate;[13] in the present work the collisional model is replaced by the physically more realistic treatment of the preexponential factor based on the "encounter preequilibrium" model.[13]

(36) This is tantamount to assuming that the classical intrinsic activation entropy ΔS^*_{int}, i.e. the activation entropy that remains in the absence of an entropic driving force, equals zero. Although this is only approximately true, generally $\Delta S^*_{int} < 10$ J K^{-1} mol^{-1} for electrochemical reactions in aqueous solution.[37]

(37) Hupp, J. T.; Weaver, M. J. *J. Phys. Chem.* **1984**, *88*, 1860.

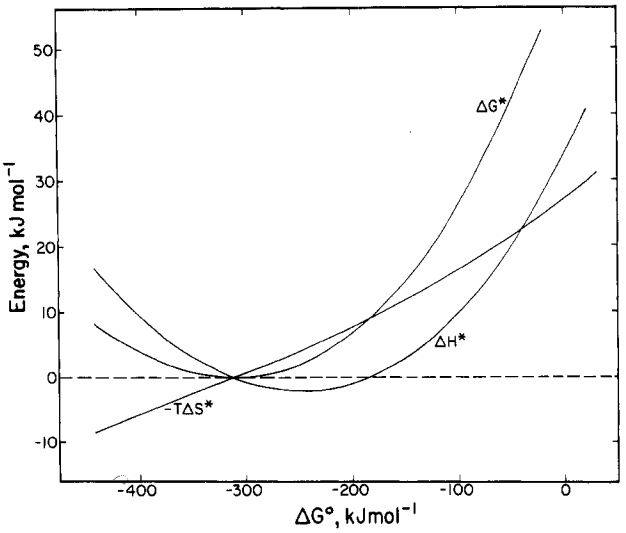

Figure 4. Calculated free energy, enthalpic, and entropic barriers, ΔG^*, ΔH^*, and $T\Delta S^*$, respectively, for $Cr(OH_2)_6^{2+}$ electrooxidation as function of free energy driving force, ΔG° ($= -F(E - E_f)$), by using eq 5, 6, 8, 11, and 13 assuming that $2\lambda_f = \lambda_r$.

Table II. The nuclear tunneling corrections to ΔH^*_{calcd} and ΔS^*_{calcd} range from ca. −3.5 to −10 kJ mol^{-1} and −7 to −22 J K^{-1} mol^{-1}, respectively, becoming more negative with increasing negative electrode potential.

Inspection of Table II reveals that the striking numerical differences in the calculated activation parameters for the anodic and cathodic directions brought about by the large reaction entropy for $Cr(OH_2)_6^{3+/2+}$ is matched to a large degree by the experimental values. This agreement extends, albeit approximately, to the very small values of ΔH^*_{cor} and ΔH^*_{calcd} for $Cr(OH_2)_6^{2+}$ oxidation at large anodic overpotentials and their mild overpotential dependence in comparison with that for $Cr(OH_2)_6^{3+}$ reduction at cathodic overpotentials. Similar calculations for $Eu(OH_2)_n^{3+/2+}$ are not feasible since the required quantitative structural data are unavailable for this couple. Nevertheless, the experimental values of ΔH^*_{cor} and ΔS^*_{cor} for $Eu(OH_2)_n^{3+/2+}$ also display striking differences in the anodic and cathodic directions as a consequence of the large ΔS°_{rc} value (195 J K^{-1} mol^{-1} [11]) for this couple. In addition, similarly small and even negative values of ΔH^*_{cor} for $Eu(OH_2)_n^{2+}$ oxidation were obtained at anodic overpotentials (e.g. $\Delta H^*_{cor} = -5$ kJ mol^{-1} at $E - E_f = 400$ mV).

An apparently unexpected finding which we alluded to earlier[1] is the observation of near-zero activation enthalpies at anodic overpotentials even though the activation entropies remain large and negative under these conditions (Table II). Intuitively, one might expect the activation entropy to equal zero in the absence of an enthalpic barrier.[1] In order to examine this matter further, values of ΔG^*_{calcd}, ΔH^*_{calcd}, and ΔS^*_{calcd} were calculated for $Cr(OH_2)_6^{2+}$ oxidation over a considerable range of free energy driving forces, ΔG°, corresponding to a much greater span of anodic overpotentials than can be examined experimentally. The resulting plots of ΔG^*_{calcd}, ΔH^*_{calcd}, and ΔS^*_{calcd} against ΔG° are given in Figure 4. (Nuclear tunneling corrections were omitted since these are small and the approximations inherent in their calculation become somewhat ambiguous for highly exoergonic reactions.[38]) Figure 4 indicates that ΔH^*_{calcd} decreases sharply and even assumes small negative values at substantially smaller driving forces than are necessary for ΔG^*_{calcd} to become zero. Indeed, ΔH^*_{calcd} attains a value of zero at two points, approximately when $\Delta G^\circ = -(\lambda_f + 2T\Delta S^\circ)$ and when $\Delta G^\circ = -\lambda_f$, whereas ΔG^*_{calcd} and ΔS^*_{calcd} become zero only when $\Delta G^\circ = -\lambda_f$. The significance of negative activation enthalpies for related homogeneous reactions has been discussed by Marcus and Sutin.[39]

A related feature of Figure 4 is the appearance of an enthalpic "inverted region", i.e. a realm of *increasing* activation enthalpy with increasing exoergonicity within the "normal free energy region", i.e. where the activation free energy decreases with increasing driving force. It has been noted that the much-discussed free energy inverted region[40] should be absent for electrochemical reactions at metal surfaces.[41,42] This is because oxidative electron transfer to metal energy states above the Fermi level, or reductive electron transfer to metal energy states above the Fermi level, or reductive electron transfer from states below the Fermi level, will provide an activationless pathway even when $-\Delta G^\circ$ exceeds λ_f. However, the *enthalpic* inverted region should nevertheless be observable for electrochemical reactions. It would be interesting to explore this possibility experimentally by selecting reactions with sufficiently negative values of ΔS° so that the anticipated enthalpic inverted region occurs at sufficiently large values of ΔG^*_{cor}, corresponding to measurably slow reaction rates.

It should be noted that the anodic–cathodic driving-force asymmetry seen for the activation parameters has a different origin than that of the rate constants discussed above. Thus, purely symmetrical Tafel plots will be predicted provided that $\lambda_f = \lambda_r$ *irrespective* of major differences in the entropic and enthalpic components of these reorganization energies.[1] Nevertheless, these two types of driving-force asymmetry are in a sense related since they both arise from equilibrium structural changes brought about by electron transfer. In addition, we have speculated that the especially small transfer coefficients observed at large anodic overpotentials (Figures 1 and 2) may be connected with the occurrence of an enthalpically barrierless process (i.e. $\Delta H^*_{cor} \sim 0$) under these conditions.[1] Although the above analysis based on force constant differences largely removes the need to invoke such "anomalous activation" mechanisms, such notions should nonetheless not be wholly discarded at this point.

Parallel Reactivity Behavior for Homogeneous and Heterogeneous Processes

The foregoing demonstrates that the chief property of simple electrochemical reactions which leads to unusual driving-force-dependent reactivities is their inherent chemical asymmetry. In this regard interfacial redox reactions have much in common with homogeneous cross-reactions between structurally diverse redox centers and in fact are more akin to these than to homogeneous self-exchange reactions. As an illustration, consider the $V(OH_2)_6^{3+/2+}$ couple. The $V(OH_2)_6^{3+/2+}$ homogeneous self-exchange reaction is a completely symmetrical process and is therefore necessarily isoenergetic as well as thermoneutral and isoentropic. In contrast, $V(OH_2)_6^{3+/2+}$ electrochemical exchange is characterized by net ΔS° and ΔH° values of −155 J K^{-1} mol^{-1} and −46 kJ mol^{-1}, respectively,[11] for the oxidation reaction at the standard potential (i.e. for $\Delta G^\circ = 0$). These thermodynamic changes are closely shared by the oxidation of $V(OH_2)_6^{2+}$ by $Cr(bpy)_3^{3+}$ in homogeneous aqueous solution (bpy = 2,2′-bipyridine), since the formal potentials of the reacting redox couples are virtually identical (−480 mV vs. SCE[11,43]) and ΔS°_{rc} for $Cr(bpy)_3^{3+/2+}$ is close to zero (15 J K^{-1} mol^{-1} [43]). (The values of ΔS° and ΔH° are deduced to be −140 J K^{-1} mol^{-1} and −41 kJ mol^{-1}, respectively.) It is not surprising, therefore, that cross-reactions between aquo and low-spin polypyridine complexes

(38) Following current thinking,[40c] the magnitude of the nuclear tunneling correction will be maximized when the enthalpic, rather than the free energy, driving force is zero. However, the relevant driving force is that associated with the particular (inner or outer shell) mode being considered. Since the partitioning of either the enthalpic or the free energy driving force into inner- and outer-shell components is fraught with difficulties, the accurate prediction of the effective dependence of Γ_n upon the cathodic and anodic overpotential is precluded at present. Nevertheless, approximate calculations for $Cr(OH_2)_6^{3+/2+}$ indicate that Γ_n depends only slightly on the overpotential increasing monotonically with increasing negative electrode potential over the range considered in Figure 1 (3.4 for $E = E_f$, 2.0 at $E - E_f = 800$ mV, and 4.0 at $E - E_f = -600$ mV).

(39) Marcus, R. A.; Sutin, N. *Inorg. Chem.* **1975**, *14*, 213.
(40) For example, see: (a) Rehm, D.; Weller, A. *Isr. J. Chem.* **1970**, *8*, 259. (b) Creutz, C.; Sutin, N. *J. Am. Chem. Soc.* **1977**, *99*, 241. (c) Siders, P.; Marcus, R. A. *J. Am. Chem. Soc.* **1981**, *103*, 748.
(41) Marcus, R. A. *J. Chem. Phys.* **1965**, *43*, 2654.
(42) Schmickler, W. *Electrochim. Acta* **1975**, *20*, 137.
(43) Sahami, S.; Weaver, M. J. *J. Electroanal. Chem. Interfacial Electrochem.* **1981**, *122*, 155.

exhibit similarly "unusual" activation parameters to electrochemical reactions involving the former reactants.[5] For example, the highly exoergonic oxidations of $Fe(OH_2)_6^{2+}$ by $Ru(bpy)_3^{3+}$, $Ru(phen)_3^{3+}$, and $Fe(phen)_3^{3+}$ are characterized by small negative activation enthalpies and large negative activation entropies.[44-46] It has been shown that the substantial negative entropic driving force for these reactions ($\Delta S^\circ \approx -175$ J K^{-1} mol^{-1} [12]) can account in broad terms for this kinetic behavior on the basis of the measured rate parameters for the parent self-exchange reactions.[39]

Moreover, comparably "anomalous" rate-driving force dependencies to those discussed here for electrochemical oxidations have also been observed for a number of homogeneous oxidations of aquo complexes.[2] Analysis of the driving-force dependencies of homogeneous reactivity is complicated by the need to account for activation of the reducing, as well as oxidizing, redox center. Low-spin polypyridine complexes provide particularly useful coreactants in this regard[2] since the small entropic changes[43] and intrinsic activation barriers[47] that are characteristic of such couples enable the reaction energetics to be dominated by the other redox center. In this respect such polypyridine reactants provide similar redox characteristics to metal surfaces. Although the "overpotential" provided by the former is fixed by its formal potential, driving-force dependencies can nevertheless be scrutinized by selecting a related series of polypyridine oxidants having a suitable range of formal potentials.[44]

The dependence of homogeneous reactivities upon the driving force has often been discussed[2,5,8,48] in terms of observed deviations from the "Marcus cross relationship"[4]

$$k_{12} = (k_{11}k_{22}K_{12}f)^{1/2} \tag{16a}$$

where

$$f = (\log K_{12})^2/[4 \log (k_{11}k_{22}/A^2)] \tag{16b}$$

Here k_{12} is the rate constant for a cross-reaction having an equilibrium constant K_{12} from the known self-exchange rate constants, k_{11} and k_{22}, for the constituent redox couples. Since eq 16 is derived by assuming that the force constants for the oxidized and reduced forms of both reacting couples are equal,[49] progressively larger deviations from this relation are expected as the driving force is increased. When $\lambda_f < \lambda_r$ (as for aquo complex oxidations), the observed values of k_{12} are expected to be progressively smaller than those predicted from eq 16 as K_{12} increases.[49] Such considerations are entirely analogous to those considered above for electrochemical reactions. Thus, the symmetrical Tafel relations obtained from the harmonic oscillator model with $\lambda_f = \lambda_r$ (eq 12) can be derived from eq 16 by noting that a metal surface can be regarded formally as a coreactant with variable driving force and zero intrinsic barrier (i.e. having a "self-exchange rate constant" equal to the preexponential factor, A).

Chou et al. regarded the deviations from eq 16 due to unequal force constants as being too small to account for the observed discrepancies for a number of homogeneous cross-reactions, including several oxidations of aquo complexes.[5] Undoubtedly other factors, such as additional components of work terms, nonadiabaticity,[5,8,48] use of inappropriate self-exchange rate constants,[50,51] etc., also contribute importantly in many cases. Nevertheless, the above analysis clearly indicates that force constant differences can provide significant driving-force-dependent deviations from eq 2 and therefore from eq 16. Indeed, by employing the free energy form of eq 16, we have demonstrated that the observed driving-force-dependent deviations observed for homogeneous oxidations of aquo complexes are quantitatively consistent with the corresponding deviations for the electrooxidation reactions that are discussed here.[2]

The present analysis focuses attention on aquo redox couples since structural as well as extensive rate parameter–overpotential data are available for these systems. Nevertheless, such rate-driving force asymmetries should be observed for any redox couple with suitably large force constant differences between the oxidized and reduced forms, providing that inner-shell reorganization provides an important contribution to the activation barrier. These two factors will tend to occur together since it is anticipated that redox couples having such large force constant differences will also exhibit sizable bond length changes upon electron transfer and hence have large inner-shell barriers. Since such large structural changes commonly give rise to rapid irreversible chemical steps following electron transfer, the number of chemically reversible couples having the required properties may be relatively small. Nevertheless, the possible occurrence of such Tafel plot asymmetry, yielding otherwise unexpected Tafel linearity or curvature, should be borne in mind when examining the electrochemical kinetics of reactions involving coupled chemical steps, including those involving proton transfer such as proton electroreduction.

Acknowledgment. We are indebted to Dr. J. K. Beattie for communicating his Raman spectral data for aquo complexes (ref 9a) prior to publication. This work is supported by the Air Force Office of Scientific Research.

Appendix. Equivalence of Eq 11 and 12

The free energy expression

$$\Delta G^* = X^2\lambda_f \tag{5a}$$

may be differentiated with respect to temperature to yield

$$\Delta S^* = -2\lambda_f X\, dX/dT \tag{A1}$$

By solving eq 5, one obtains for X

$$X = \{-\lambda_r + [\lambda_r^2 + (\lambda_f - \lambda_r)(\Delta G^\circ + \lambda_r)]^{1/2}\}(\lambda_f - \lambda_r)^{-1} \tag{A2}$$

If one assumes that $d\lambda/dT = 0$, differentiation of eq A2 yields

$$dX/dT = -\tfrac{1}{2}\Delta S^\circ[\lambda_r^2 + (\lambda_f - \lambda_r)(\Delta G^\circ + \lambda_r)]^{-1/2} \tag{A3}$$

Substitution of eq A3 into eq A1 yields

$$\Delta S^* = \Delta S^\circ X\lambda_f[\lambda_r^2 + (\lambda_f - \lambda_r)(\Delta G^\circ + \lambda_r)]^{-1/2} \tag{11}$$

Rearranging eq A2, we find that

$$[\lambda_r^2 + (\lambda_f - \lambda_r)(\Delta G^\circ + \lambda_r)]^{1/2} = X(\lambda_f - \lambda_r) + \lambda_r \tag{A4}$$

and

$$[\lambda_r^2 + (\lambda_f - \lambda_r)(\Delta G^\circ + \lambda_r)]^{-1/2} = (X\lambda_f + \lambda_r - X\lambda_r)^{-1} \tag{A5}$$

Incorporating this result into eq 11 yields

$$\Delta S^* = \Delta S^\circ\lambda_f X(X\lambda_f + \lambda_r - X\lambda_r)^{-1} \tag{A6}$$

From eq 5b one can obtain (noting that $d\lambda/dX = 0$)

$$d\Delta G^\circ/dX = 2(X\lambda_f + \lambda_r - X\lambda_f) \tag{A7}$$

From eq 5a one finds that

$$d\Delta G^*/dX = 2X\lambda_f \tag{A8}$$

In view of eq A7 and A8, eq A6 may be rewritten as

$$\Delta S^* = \Delta S^\circ(d\Delta G^*/dX)(d\Delta G^\circ/dX)^{-1} = \Delta S^\circ\, d\Delta G^*/d\Delta G^\circ \tag{A9}$$

Noting that the transfer coefficient α is defined as $d\Delta G^*/d\Delta G^\circ$, we recover the simple expression

$$\Delta S^* = \alpha\Delta S^\circ \tag{12a}$$

At first sight, eq 12a appears to be simply the entropic analogue of the free energy expression

$$\Delta G^* = \Delta G^*_{int} + \alpha\Delta G^\circ \tag{A10}$$

where ΔG^*_{int} is the intrinsic free energy barrier, i.e. that which

(44) Sutin, N.; Gordon, B. M. *J. Am. Chem. Soc.* **1961**, *83*, 70.
(45) Braddock, J. N.; Meyer, T. J. *J. Am. Chem. Soc.* **1973**, *95*, 3158.
(46) Cramer, J. L.; Meyer, T. J. *Inorg. Chem.* **1974**, *13*, 1250.
(47) Brown, G. M.; Sutin, N. *J. Am. Chem. Soc.* **1979**, *101*, 883.
(48) Weaver, M. J.; Yee, E. L. *Inorg. Chem.* **1980**, *19*, 1936.
(49) Newton, T. W. *J. Chem. Educ.* **1968**, *45*, 571.
(50) Endicott, J. F.; Durham, B.; Kumar, K. *Inorg. Chem.* **1982**, *21*, 2437.
(51) Hupp, J. T.; Weaver, M. J. *Inorg. Chem.* **1983**, *22*, 2557.

remains in the absence of the free energy driving force $\Delta G°$. (Equation A10 is the most general form of the dependence of the activation barrier upon the driving force.) Indeed, the above assumption, $d\lambda/dT = 0$, made in deriving eq 12a is equivalent to asserting that the intrinsic entropic barrier equals zero. However, a difference between the forms of eq 12a and A10 is that the transfer coefficient appearing in the former is the usual *differential* quantity, α_d, defined in eq 1 or, equivalently, by $\alpha_d = d\Delta G^*/d\Delta G°$, whereas that occurring in the latter is an *integral* quantity defined by $\alpha_i = (\Delta G^* - \Delta G^*_{int})/\Delta G°$. Generally α_d will differ from α_i when the Tafel plots are curved, i.e. when α depends upon $\Delta G°$.[3] This distinction between the forms of eq 12a and A10 arises since the former can be obtained by taking the temperature derivative of the latter at a constant Galvani potential (i.e. nonisothermal cell potential), whereupon $d\alpha_i/dT \neq 0$.

Registry No. $Cr(OH_2)_6^{3+}$, 14873-01-9; $Cr(OH_2)_6^{2+}$, 20574-26-9; mercury, 7439-97-6.

Aluminum-27 and Phosphorus-31 Nuclear Magnetic Resonance Studies of Aluminophosphate Molecular Sieves

C. S. Blackwell* and R. L. Patton

Union Carbide Corporation, Tarrytown, New York *(Received: May 4, 1984)*

The ^{27}Al NMR and ^{31}P NMR MAS spectra of four crystalline aluminophosphate molecular sieves, $AlPO_4$-5, $AlPO_4$-11, $AlPO_4$-17, and $AlPO_4$-31 were studied at 4.7 T and compared to some nonmicroporous materials, $AlPO_4$-quartz, metavariscite, and $AlPO_4$-tridymite. The molecular sieve spectra are generally consistent with their known framework structures constructed of alternating AlO_4 and PO_4 tetrahedra; however, the ^{27}Al NMR chemical shift range was wide and asymmetrical lines and multiple peak maxima were observed. Both as-synthesized and calcined forms were examined and in one case ($AlPO_4$-17) adsorbed water reversibly resulted in a chemical shift into a region previously found from octahedral Al in aluminophosphates and herein from metavariscite. High fields (9.4 T) and $\{^1H$-$^{27}Al\}$ cross-polarization techniques helped assign the most unusual ^{27}Al NMR chemical shifts to the result of secondary interactions of framework Al with occluded template or H_2O within the micropores. Quadrupole effects are so severe in $AlPO_4$-quartz that even at 9.4 T a residual powder pattern persists under MAS conditions. All the ^{31}P NMR MAS results are consistent with tetrahedral phosphorus.

Introduction

Many previous researchers[1-6] have shown that ^{27}Al NMR chemical shifts can be correlated with the coordination number of aluminum in Al–O compounds. High-field NMR, made possible by superconducting magnets, can be used to increase chemical shift dispersion and reduce second-order quadrupole coupling effects. MAS (magic angle spinning) can further reduce second-order quadrupole effects (by a factor ca. 3) as well as often remove both CSA (chemical shift anisotropy) and dipole–dipole effects.

High-resolution ^{27}Al NMR MAS spectra have been obtained for crystalline aluminum oxides,[1,2] aluminosilicates,[4,7] aluminosilicate glasses,[8,9] and nonmicroporous aluminophosphates.[10] We now report initial solid-state NMR studies of four members of the newly discovered family of synthetic, crystalline aluminophosphate molecular sieves first reported by Wilson et al.[11] Several of these microporous $AlPO_4$ frameworks are zeolite structural analogues, but most are novel and the crystal structure of one, $AlPO_4$-5, was described by Bennett et al.[12] The known structures can, like the zeolites, be described as three-dimensional tetrahedral framework oxides. The Al and P atoms alternate, each surrounded by four framework oxygens to form $Al(OP)_4$ or $P(OAl)_4$ linkages, respectively.

Experimental Section

The NMR spectra were obtained on a Bruker CXP-200 solid-state and high-resolution NMR spectrometer operating at a field of 4.7 T with a standard ^{13}C cross-polarization magic angle spinning (CP-MAS) accessory probe. Additional spectra were also taken on a Bruker AM-400 (9.4 T). The ^{31}P NMR chemical shifts are referred to external H_3PO_4 (85%) and the ^{27}Al NMR chemical shifts are referred to external $Al(H_2O)_6^{3+}$ in $Al(NO_3)_3$ aqueous solution.[13] Recalibration for magnet drift was done daily; changes of only a few hertz back and forth were observed. The chemical shift calibration is reproducible to less than 0.1 ppm, but when applied to samples is subject to bulk susceptibility effects. The Andrews-Beam single bearing rotors were made of Delrin and spun with dry nitrogen at approximately 3–4 kHz; extensive spinning sidebands could be seen when quadrupole effects were large. The magic angle was adjusted by maximizing the spinning sidebands[15] for the ^{79}Br NMR resonance of ^{79}Br in KBr. A typical ^{31}P NMR spectrum was obtained from Bloch decay experiments of 20–1000 co-added fid's (free induction decays) produced by 4-μs pulses followed by a 60-s relaxation delay. For ^{27}Al NMR typically 500–1000 Block decay fid's were accumulated by using

(1) Muller, D.; Gessner, W.; Grimmer, A. R. *Z. Chem.* **1977**, *17*, 453.
(2) Muller, D.; Gessner, W.; Behrens, H.-J.; Scheler, G. *Chem. Phys. Lett.* **1981**, *79*, 59.
(3) Mastikhin, V. M.; Krivorochko, O. P.; Zolotovski, B. P.; Buyanov, R. A. *React. Kinet. Catal. Lett.* **1981**, *18*, 117.
(4) Freude, D.; Behrens, H.-J. *Cryst. Res. Technol. (1979-)* **1981**, *16*, K36.
(5) Lampe, F. v.; Muller, D.; Gessner, W.; Grimmer, A.-R.; Scheler, G. *Z. Anorg. Allg. Chem.* **1982**, *489*, 16.
(6) de Jong, B. H. W. S.; Schramm, C. M.; Parziale, V. E. *Geochim. Cosmochim. Acta* **1983**, *47*, 1223.
(7) Fyfe, C. A.; Gobbi, G. C.; Hartman, J. S.; Klinowski, J.; Thomas, J. M. *J. Phys. Chem.* **1982**, *86*, 1247.
(8) Muller, D.; Hoebbel, D.; Gessner, W. *Chem. Phys. Lett.* **1981**, *84*, 25.
(9) Hallas, E.; Haubenreisser, U.; Hahnert, M.; Muller, D. *Glastech. Ber.*, in press.
(10) Muller, D.; Grunze, I.; Hallas, E.; Ludwig, G. *Z. Anorg. Allg. Chem.* **1983**, *500*, 80.
(11) (a) Wilson, S. T.; Lok, B. M.; Messina, C. A.; Cannan, T. R.; Flanigen, E. M. *J. Am. Chem. Soc.* **1982**, *104*, 1146. (b) Wilson, S. T.; Lok, B. M.; Messina, C. A.; Cannan, T. R.; Flanigen, E. M. In "Intrazeolite Chemistry"; American Chemical Society: Washington DC, 1983; *ACS Symp. Ser.* No. 218, p 79.
(12) Bennett, J. M.; Cohen, J. P.; Flanigen, E. M.; Pluth, J. J.; Smith, J. V. In "Intrazeolite Chemistry"; American Chemical Society: Washington, DC, *ACS Symp. Ser.* No. 218, p 109.
(13) Since aluminum chloride solutions can have very complex compositions due to hydrolysis,[14] we chose instead to use aqueous $Al(NO_3)_3$, reputed to remain unassociated, to generate a resonance for $Al(H_2O)_6^{3+}$ as our 0 ppm reference.
(14) Cotton, F. A.; Wilkinson, G. C. "Advanced Inorganic Chemistry"; Wiley-Interscience: New York, 1972; p 266.
(15) Frye, J. S.; Maciel, G. E. *J. Magn. Reson.* **1982**, *48*, 125.

0022-3654/84/2088-6135$01.50/0